Enhanced finite control set-model predictive control for three-phase split-source inverters

Bakeer, Abualkasim ; Dabour, Sherif M.; Gowaid, I.A.; Aboushady, Ahmed A.; Elgenedy, Mohamed A.; Farrag, Mohamed Emad

Published in:
2022 57th International Universities Power Engineering Conference

DOI:
10.1109/UPEC55022.2022.9917867

Publication date:
2022

Document Version
Author accepted manuscript

Enhanced Finite Control Set-Model Predictive Control for Three-Phase Split-Source Inverters

Abualkasim Bakeer[1], Sherif M. Dabour[2,3,(*)], I. A. Gowaid[3], A. Aboushady[3], M. A. Elgenedy[3], and Mohamed Emad Farrag[3]
[1]*Department of Electrical Engineering, Faculty of Engineering, Aswan University, Aswan 81542, Egypt*
[2]*Faculty of Engineering, Tanta University, Tanta, Egypt, 31733, Egypt*
[3]*School of Computing, Engineering, and Built Environment, Glasgow Caledonian University, Glasgow, UK, G4 0BA*
[(*)]Sherif.Dabour@gcu.ac.uk

***Abstract*—Three-phase Split-source inverter (SSI) has recently been proposed as an alternative to the three-phase Z-source inverters (ZSI). This paper introduced an improved finite control set-model predictive control (FCS-MPC) algorithm for the SSI. The proposed FCS-MPC algorithm reduces the computational burden by selecting the discharging vector directly according to the current status of the inductor compared to its reference point instead of checking the other states. Moreover, it simplifies the cost function by removing the inductor current term, and thus no weighting factor is needed inside the cost function. A detailed analysis of the proposed algorithm is presented in this paper. Finally, simulation results based on MATLAB have been introduced to show the viability of the presented research and theoretical study of the FCS-MPC algorithm of the three-phase SSI under different operating conditions.**

Keywords—Split-source inverter, Model predictive control, Cost function definition, Single-stage boosting inverter.

I. INTRODUCTION

WITH one stage, the single-stage inverters can increase or decrease the output ac voltages that are synthesized from the dc-supplies. Many types have been developed for these inverters in the last two decades. These types use the passive components (inductors and capacitors) in conjunction with the semiconductors to perform the bucking/boosting and the dc-ac inversion processes [1]. It can be categorized into three basic configurations called impedance source-based inverters (ZSI), differential-mode inverters (DMI), and split source inverters (SSI). According to their structures and general characteristics, these basic configurations are divided into several categories [1]. Due to its superior features, the split-source inverter (SSI), shown in Fig. 1, has proven to be the most attractive single-stage inverter topology [2]. As shown in Fig. 1, the SSI has a simple structure to its counterparts. It requires a lower passive component count. Typically, it combined the conventional dc-dc boost converter with the standard six-switch full-bridge (B6) three-phase voltage source inverter (VSI) in one circuit. Therefore, it uses only one inductor and one capacitor on the dc-side. It also has continuous input current and dc-link voltage. Moreover, it utilizes the switching vectors of the standard VSI, shown in Fig. 2, for both the boosting and inversion actions.

There have been numerous studies on SSI [3-11]. Some research work has focused on extending the concept of the two-level three-phase SSI to the multilevel topologies to enhance the quality of the output voltages. The topologies of flying diodes, flying capacitors, and cascaded approaches are introduced in [3]-[7]. In [8], the SSI concept is applied to the nine-switch inverter topology to obtain two independent three-phase groups in the output with high voltage gains from a single low voltage dc-source. Another research effort has concerns about improving the boosting capabilities of the SSI topology. The proposed topologies in [9]-[14] extend the switched impedance concepts used for dc-dc converters, Z-source, and Y-source inverters to increase the SSI output voltages using additional input passive elements.

Moreover, other studies have introduced the applications of the SSI for renewable energy conversion systems, especially photovoltaic (PV) and wind turbine converters. Several studies have been developed to integrate SSI into grid-connected renewable energy sources [15]-[18]. A decoupled control approach with a modified modulation technique connects the SSI to the three- and single-phase grids in [15],[16], respectively. The cascaded proportional-resonant and proportional-integral control scheme guarantee zero steady-state error for both ac and dc sides of the single-phase SSI [17]. Detailed design procedures for a standalone SSI-based PV system with a battery storage system are presented in [18]. These control approaches have several shortcomings, among them inadequate responses and complexity.

Recent attention to the control of power converters has been directed to MPC as a more advanced control theory. The MPC algorithm generally uses a system model to predict its future behaviour and a cost function that should first be defined based on the expected targets for control based on an optimality criterion [19]. To our knowledge, few studies have yielded on the application of MPC for SSI topology [20]-[25]. The finite control set MPC method for SSI connected to the grid is proposed in [20] and for standalone configurations in [21]-[23]. A virtual synchronous generator-based MPC for grid-connected SSI is presented in [24]. The cost function for the SSI is typically formulated by combining the system state errors (inductor current, capacitor voltage, and output currents) with appropriate weighting factors. The weighting factors in the methods mentioned above are determined by trial-and-error and heuristic methods. This approach is complicated, cumbersome, and time-consuming. It makes the problem challenging to implement in real-time. A solution to this problem is proposed in [25] using energy-function based model predictive control (EF-MPC). However, this method is applied for single-phase SSI topology.

This paper proposes a solution to the problem of determining the weighting factors for the three-phase SSI topology. The proposed algorithm simplifies the cost function by removing the inductor current term, and thus no weighting factor is needed inside the cost function. Moreover, the proposed MPC algorithm reduces the computational burden by selecting the discharging vector directly according to the current status of the inductor compared to its reference point. A detailed analysis of this algorithm is introduced. In addition, simulation results have been presented to show the viability of the proposed research and theoretical study of the MPC algorithm of the three-phase SSI under different conditions.

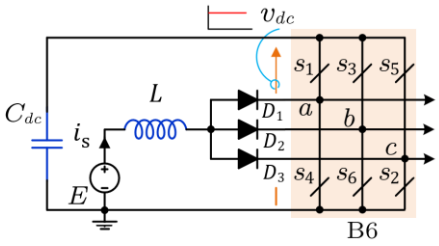

(a) Basic SSI topology.

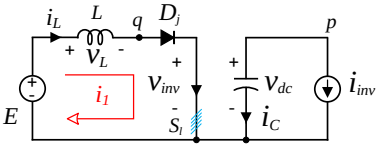

(b) Inductive charging (for states V_0-V_6).

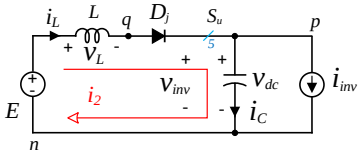

(c) Inductive discharging (for state V_7).

Fig. 1. Split-source inverter [14].

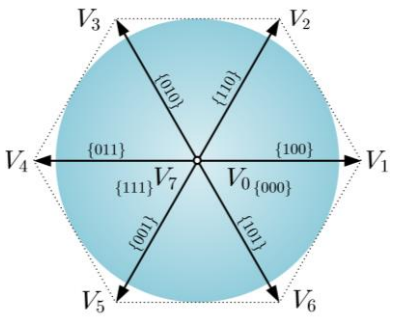

Fig. 2. Space vector model of SSI.

II. Three-Phase Split-Source Inverters

A. Topology

The three-phase SSI topology is shown in Fig. 1. This topology is acquired by combining a dc-dc boost converter into the VSI bridge (B6). This can be done by connecting a boost inductor, L, to the midpoint of each leg of the inverter (a, b, c) via the forward diodes (D_1-D_3).

B. Operation

Since the three-phase SSI utilizes the B6 bridge of the standard VSI, therefore, it uses the same switching vectors ($V_o - V_7$), shown in Fig. 2 [20]-[24]. The inductor, L, and the diodes of Fig. 1 are used to boost the supply voltage to the desired dc-link voltage at the capacitor, C_{dc}.

It is important to note that the three-phase SSI uses the switching vectors $V_o - V_6$ to charge the input inductor, while the remaining zero vector V_7 is used to discharge the inductive energy to the dc-link capacitor. The equivalent circuits of both inductive charging and discharging modes are shown in Fig. 1(b) and (c).

1) Inductive Charging Mode: The charging mode can be obtained by switching ON at least one of the lower switches in the B6 bridge. In this case, the voltage at the output of the dc-side is zero (i.e. $v_{inv} = 0$) due to the short circuit, as shown in Fig. 1(b). As a result, the inductor L is charged.

2) Inductive Discharging Mode: The discharging mode only occurs when all the upper switches in the B6 bridge are turned ON. In this case, the inductor L will discharge its energy in the capacitor C via the antiparallel diodes of the upper switches. Hence, the voltage at the dc-side equals the capacitor voltage (i.e. $v_{inv} = v_{dc}$), as shown in Fig. 1(c).

C. Boosting Factor and AC Voltage Gain

The ratio between the dc-link voltage, v_{dc} (that is, capacitor voltage) to the supply voltage, E is defined as the dc-boosting factor β, which can be expressed as follows [9]

$$\beta = 1/(1 - D_{av}) \tag{1}$$

where D_{av} is the average dc-boosting duty cycle of the inductive charging interval during the complete switching period, T_{sw}. Finally, the output ac voltage gain, G is governed by

$$G = \frac{\hat{V}_1}{E} = \frac{\beta M}{2\sin(\pi/3)} = \frac{M}{2\sin(\pi/3)\,(1 - D_{av})} \tag{2}$$

where $\hat{V}_1$ is the peak value of the fundamental component of the output phase voltage, and M is the modulation index.

III. Proposed Finite Control Set-Model Predictive Control for SSI

The complete block diagram of the proposed FCS-MPC for three-phase SSI is shown in Fig. 3. The FCS-MPC is considered an optimal switching state prediction model with a receding horizon. Thus, the first step is to establish a discrete-time model of the control objectives at the k^{th} sampling instant, then predicts the future load and inductor currents from the dc-link voltage and their measured values, as shown in Fig. 3.

A. Discrete Modeling of the Control Objectives

1. RL Load Current

For every possible output voltage of the SSI, the magnitude of the future load current, $i_o(k+1)$ is calculated as follows

$$i_o(k+1) = \frac{T_s V_x(k+1) + L_o i_o(k)}{L_o + R_o T_s} \tag{3}$$

where $i_o(k)$ is the load current space vector at the k^{th} sampling instant, T_s is the sampling interval, R_o & L_o are the resistance and inductance of the load, respectively, and $V_x(k+1)$ is the space vector of the output voltage, which can be determined from (4) and Table I for each switching state combination.

$$V_x(k+1) = \frac{2}{3} v_{dc}(S_1 + aS_3 + a^2 S_5) \tag{4}$$

where $a = e^{j2\pi}$.

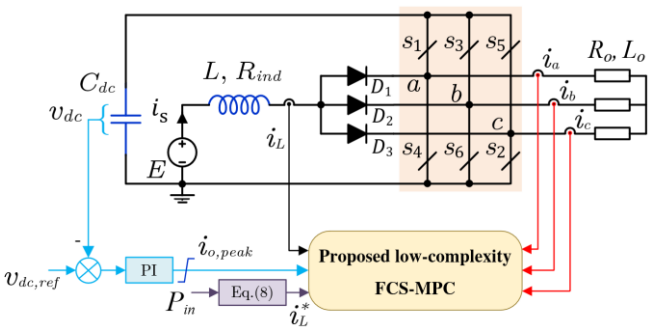

Fig. 3. The complete structure of the proposed FCS-MPC of SSI.

TABLE I. POSSIBLE SSI SWITCHING PATTERNS.

n	V_x	S_1	S_4	S_3	S_6	S_5	S_2	L status
1	V_0	0	1	0	1	0	1	Charging with the same slope
2	V_1	1	0	0	1	0	1	
3	V_2	1	0	1	0	0	1	
4	V_3	0	1	1	0	0	1	
5	V_4	0	1	1	0	1	0	
6	V_5	0	1	0	1	1	0	
7	V_6	1	0	0	1	1	0	
8	V_7	1	0	1	0	1	0	Discharging

2. *Input Inductor Current*

As an illustration of how the proposed MPC strategy works on the dc-side, Fig. 4 provides the inductor's current trajectory. As shown in Fig. 4, the inductor current has two states. It increases during the charging process, which is related to the switching vectors $V_0 - V_6$ and decreases during the discharging period or at applying the zero vector V_7.

Based on the equivalent circuits of Fig. 1(b-c), the predicted current of the inductor $i_L(k+1)$ can be calculated in charge mode with the following formula

$$i_L(k+1) = \frac{T_s E + L i_L(k)}{L + R_{ind} T_s} \tag{5}$$

where E is the input voltage, L is the inductance value of the input inductor, and R_{ind} is the equivalent series resistance (i.e., ESR) of the inductor L.

In discharge mode, the predicted inductor current can be formulated as follows

$$i_L(k+1) = \frac{T_s(E - v_{dc}(k)) + L i_L(k)}{L + R_{ind} T_s} \tag{6}$$

B. *Reference Calculations*

In the proposed technique, the voltage of the dc-link capacitor is regulated via a linear proportional-integral (PI) controller at its set point, $v_{dc,ref}$. In this way, the saturation block can limit the maximum load current. The saturation limits are determined according to the converter design. As a result, we can define the three-phase load current peak as in (7), where s is the Laplace operator and k_p and k_i are the proportional and integral gains of the PI controller. Furthermore, it is possible to calculate the inductor current reference using the desired power from the source (Pin) and the input voltage as in (8).

$$i_{o,peak}(k+1) = \left(k_p + k_i s\right)\left(v_{dc,ref} - v_{dc}(k)\right) \tag{7}$$

$$i_L^*(k+1) = \frac{P_{in}}{E} \tag{8}$$

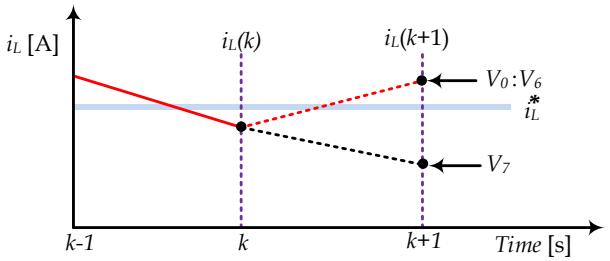

Fig. 4. Inductor current trajectory during charging and discharging states.

C. *Proposed Powerful FCS-MPC Algorithm for SSI*

The basic idea behind the proposed control algorithm is to check the state of the inductor current directly, i_L if it needs to charge or release its energy into the dc-link capacitor at the next sampling time, aiming to be close to its desired set point. As mentioned above, the inductive charging switching vectors $(V_0 - V_6)$ allows i_L to be increased with the same slope. This can be observed from the prediction equation (5) of i_L. It is not a function of the switching vector. On the contrary, the inductor has a single discharge switching vector of V_7 as can be shown in Table I.

The flowchart of the proposed FCS-MPC of SSI is depicted in Fig. 5. The algorithm begins with measuring the state variables of i_L, v_{dc}, and i_{abc} at the current instant of k^{th}. Then, $i_L(k+1)$ is calculated when one of the seven charging switching vectors is applied based on (5), and in case, the discharging vector is applied to the SSI switches using (6).

For each predicted value, the cost function is evaluated using a single cost function as in (9) to determine which state of i_L is close to the reference value of i_L^*.

$$g_L = |i_L^*(k+1) - i_L(k+1)| \tag{9}$$

If the value of the discharging state's cost function (i.e., g_{dch}) is the same or lower than the charging state's cost function (i.e., g_{ch}), then the discharging switching vector V_7 should be directly applied to the SSI switches to make the inductor current as close to its setpoint. This will be the optimal switching vector for i_L and allows it to be closer to the reference value. By doing this, the FCS-MPC algorithm does not require further calculations for the load current over checking the seven charging states (i.e., V_0-V_6). Hence, the burden of FCS-MPC calculations to find the optimal switching vector in the next sampling interval can be reduced.

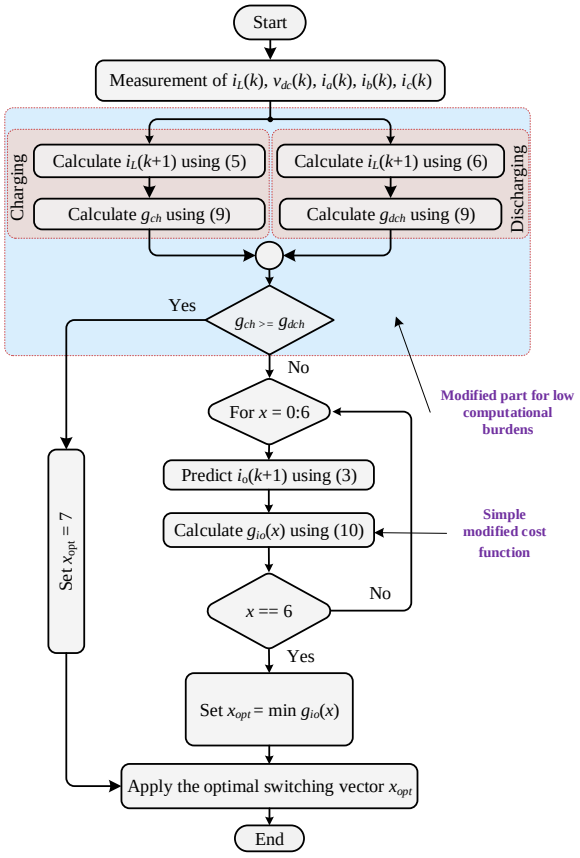

Fig. 5. Complete flowchart of the low-complexity FCS-MPC of SSI.

Otherwise, the FCS-MPC algorithm should determine which charging vector (i.e., $V_0 - V_6$) is needed at the next sampling time to make the current of the load as close as possible to its setpoint. This can be done by evaluating the cost function for the predicted load current at each vector as in (10). It can be noted that the load current's cost function has a single term, so it does not need a weighting factor that can not be defined using a direct formula [26]. While the conventional cost function has two terms (see Eq. 11), which need the weighting factor to penalize their priority in the control actions during the next sampling time.

$$g_{io} = |i_o^*(k+1) - i_o(k+1)| \quad (10)$$

$$g_{io} = |i_o^*(k+1) - i_o(k+1)| + \lambda |i_L^*(k+1) - i_L(k+1)| \quad (11)$$

IV. Simulation Results

Based on the above analysis, the MATLAB® software platform was used to implement the three-phase SSI using the proposed low complexity MPC method. MATLAB script containing the whole MPC algorithm, described in Fig. 5, is interfaced with the Simulink model to control the operation of the inverter switches. We first read the inductor current, dc-link voltage, and the output three-phase currents in the script. Then, the inductor current is predicted for both charging and discharging operations. After that, the optimal vector is selected. The inverter is loaded by a three-phase inductive load and supplied from a constant dc-source. Simulations were performed according to the parameters outlined in Table II. Two different scenarios are conducted to investigate the system performance, and the results are shown in Figs. 6-9. It is important to note that the inverter circuit is assumed to be ideal in all cases. Hence, the inverter input and output power are the same.

A. Step change of the power

In this case, the reference of the input power, P_{in} (or approximately the output power), is stepped from 1 to 0.5 kW at a time of 0.1 second, while the input dc voltage is assumed to be fixed at 100 V. Therefore, according to the block diagram in Fig. 3, the input current reference will be changed from 10 to 5 A. Fig. 6 shows the obtained simulation results. The results in Fig. 6(a) indicate that the inductor current drawn from the supply tracks the reference current waveform with a good dynamic response.

Moreover, the voltage of the dc-link capacitor restores its initial value after the disturbance without oscillation, as shown in Fig. 6(b). The dc-link capacitor voltage ripple has been reduced after reducing the power. In addition, a fast response is observed for the load currents with near sinusoidal waveforms, as depicted in Fig. 6(c).

TABLE II. Simulation Parameters of the Proposed FCS-MPC for SSI.

Parameter	Symbol	Value
Input voltage	V_{in}	100 V
SSI inductor	$\boldsymbol{L}$	4 mH
SSI ESR of the inductor	$\boldsymbol{R_{ind}}$	100 mΩ
SSI dc-link capacitor	C_{dc}	600 µF
Load resistance	$\boldsymbol{R_o}$	37 Ω /phase
Load inductance	$\boldsymbol{L_o}$	15 mH/phase
Dc-link voltage reference	$V_{dc,ref}$	425 V
Sampling time	T_s	25 µs

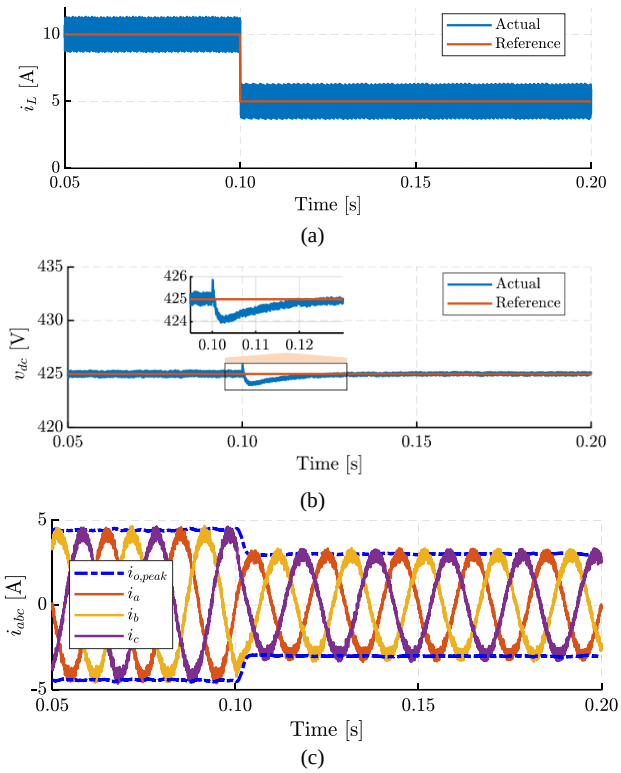

Fig. 6. Simulation results for the SSI based on the proposed FCS-MPC with a 50% step change in load (input) power at an instant of 0.1 s.

Fig. 7 shows the Fast Fourier Transform (FFT) spectrum for the load current based on the proposed algorithm at an input power 1 kW. It can be seen that the output current has lower THD, and the inverter switches are operated at an average switching frequency of approximately 1kHz.

B. Step change of the supply voltage

In this scenario, a simulation study for a step-change by 50% of the supply voltage while the input/output power remains constant at 1 kW is investigated, as shown in Fig. 8.

Fig. 9 shows the selection of optimal switching vector, while Table III lists a comparison between the proposed FCS-MPC and the conventional approach presented in [20] to validate the effectiveness of the proposed method for reducing the computational burdens of SSI for approximately three sampling intervals. The optimal switching vectors are assumed to be selected twice as a charging vector and the third time as a discharging vector. It can be observed that the proposed algorithm reduces the computational burden by 55% more than the conventional algorithm. This is owed to the selection of the discharging vector directly according to the inductor current status compared to its reference point instead of checking the other states. This results in simplifying the cost function.

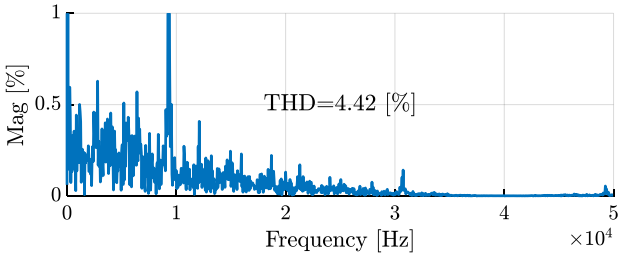

Fig. 7. FFT spectrum of the load current based on the proposed FCS-MPC of SSI at an input power of 1 kW.

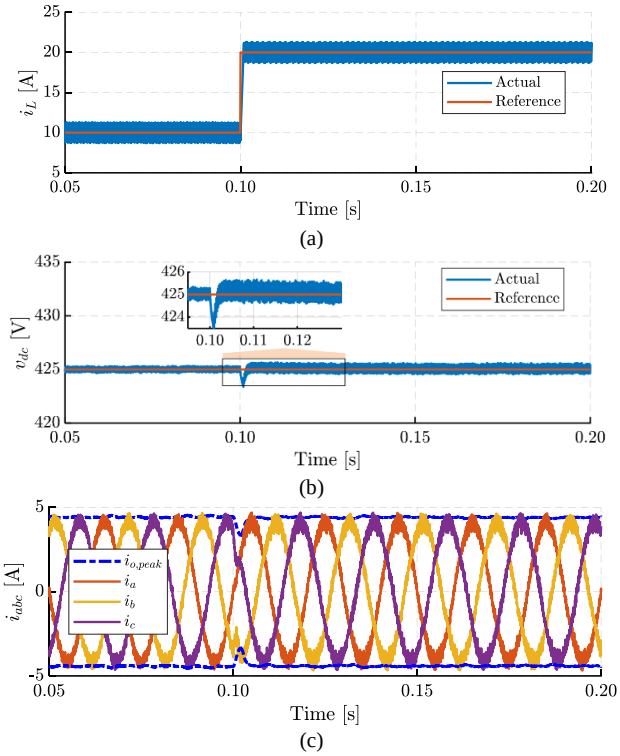

Fig. 8. Simulation results for the SSI based on the proposed FCS-MPC algorithm with a 50% input voltage step change at the instant of 0.1s.

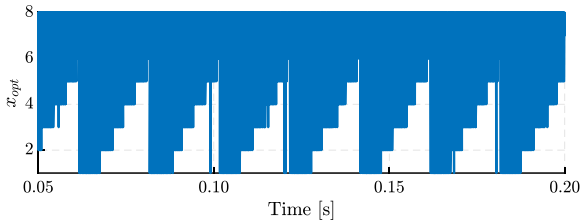

Fig. 9. Proposed FCS-MPC optimal switching vector ($n = x_{opt}$).

TABLE III. COMPARISON OF CALCULATION BURDENS BETWEEN THE CONVENTIONAL AND PROPOSED FCS-MPC OF SSI FOR APPROXIMATELY THREE SAMPLING INTERVALS.

Equation	Conventional FCS-MPC [20]	Proposed FCS-MPC
3	3 × 8	2 × 7
4	3 × 8	2 × 7
5	3 × 7	3 × 1
6	3 × 1	3 × 1
9	3 × 8	3 × 2
10	3 × 8	2 × 7
Total (%)	120 (100%)	54 (45%)

V. CONCLUSIONS

This paper enhances the algorithm of FCS-MPC for SSI topology by reducing its computational burden. This reduction is made by selecting the discharging vector of the SSI from the inductor current directly instead of the cost function. Therefore, there is no need to use the weighting factors, and the cost function is simplified to just one term. The operating principle and the mathematical analysis of the proposed method are presented. Simulation studies are conducted to validate the theoretical analysis. The results provide excellent and fast dynamic responses with a 55% reduction of the computational burden compared to the conventional algorithm.

Moreover, the results show that the actual and reference inductor currents are identical for all cases. In addition, the algorithm controls the voltage of the dc-link capacitor and the load currents. The future work related to the paper could be integrating the dc-link voltage control into the proposed FCS-MPC.

REFERENCES

[1] M. Azizi, O. Husev, D. Vinnikov, "Single-Stage Buck-Boost Inverters: A State-of-the-Art Survey," *Energies*, vol. 15, pp. 1-16, 2022.

[2] A. Abdelhakim, P. Mattavelli, and G. Spiazzi, "Three-Phase Split-Source Inverter (SSI): Analysis and Modulation," in IEEE Transactions on Power Electronics, vol. 31, no. 11, pp. 7451-7461, Nov. 2016.

[3] A. Abdelhakim and P. Mattavelli, "Analysis of the three-level diode-clamped split-source inverter," IECON 2016 - 42nd Annual Conference of the IEEE Industrial Electronics Society, 2016, pp. 3259-3264, doi: 10.1109/IECON.2016.7793581.

[4] A. Abdelhakim, P. Mattavelli, and G. Spiazzi, "Three-Phase Three-Level Flying Capacitors Split-Source Inverters: Analysis and Modulation," in IEEE Transactions on Industrial Electronics, vol. 64, no. 6, pp. 4571-4580, June 2017, doi: 10.1109/TIE.2016.2645501.

[5] M. AbdulSalam, S. M. Dabour, and E. M. Rashad, "Cascaded Multilevel Split-Source Inverters: Analysis and Modulation," 2019 21st International Middle East Power Systems Conference (MEPCON), 2019, pp. 1204-1209, doi: 10.1109/MEPCON47431.2019.9008050.

[6] S. H. Montazeri, J. Milimonfared and M. Zolghadri, "A New Modeling and Control Scheme for Cascaded Split-Source Converter Cells," in IEEE Transactions on Industrial Electronics, vol. 69, no. 8, pp. 7618-7628, Aug. 2022, doi: 10.1109/TIE.2021.3111559.

[7] S. H. Montazeri, J. Milimonfared and M. R. Zolghadri, "Multidimensional Pulse Width Modulation for Cascaded Split-Source Inverter," in IEEE Transactions on Industrial Electronics, doi: 10.1109/TIE.2022.3150087.

[8] S. M. Dabour, A. S. Abdel-Khalik, S. Ahmed and A. Massoud, "An Optimal PWM Technique for Dual-Output Nine-Switch Boost Inverters With Minimum Passive Component Count," in IEEE Transactions on Power Electronics, vol. 36, no. 1, pp. 1065-1079, Jan. 2021, doi: 10.1109/TPEL.2020.3001372.

[9] M. Chen, C. Yin and P. C. Loh, "Magnetically Coupled High-Voltage-Boost Split Y-Source Inverter Without Leakage-Induced Voltage Spikes," in IEEE Transactions on Industrial Electronics, vol. 67, no. 7, pp. 5444-5455, July 2020, doi: 10.1109/TIE.2019.2931227.

[10] X. Fang, W. Zhang, X. Kan, and Q. Wang, "Three-Phase Split Delta-Source Inverter: Operating Principles and Modulation," 2020 IEEE 3rd Student Conference on Electrical Machines and Systems (SCEMS), 2020, pp. 775-780, doi: 10.1109/SCEMS48876.2020.9352323.

[11] P. M. Kishore, A. Sabnaveesu and R. Bhimasingu, "High Gain Switched Inductor Split Source Inverter for Solar Energy Applications," 2020 IEEE 9th Power India International Conference (PIICON), 2020, pp. 1-6, doi: 10.1109/PIICON49524.2020.9113024.

[12] F. Akbar, H. Cha, H. F. Ahmed, and A. A. Khan, "A Family of Single-Stage High-Gain Dual-Buck Split-Source Inverters," in IEEE Journal of Emerging and Selected Topics in Power Electronics, vol. 8, no. 2, pp. 1701-1713, June 2020, doi: 10.1109/JESTPE.2019.2894384.

[13] M. Wageh, S. M. Dabour, and R. M. Mostafa, "A High Gain Split-Source Inverter with Reduced Input Current Ripple," 2021 22nd International Middle East Power Systems Conference (MEPCON), 2021, pp. 383-388, doi: 10.1109/MEPCON50283.2021.9686237.

[14] S. M. Dabour et al., "Modeling and Control of Single-Stage Quadratic-Boost Split Source Inverters," in IEEE Access, vol. 10, pp. 24162-24180, 2022, doi: 10.1109/ACCESS.2022.3153510.

[15] A. Abdelhakim, P. Mattavelli, V. Boscaino, and G. Lullo, "Decoupled Control Scheme of Grid-Connected Split-Source Inverters," in IEEE Transactions on Industrial Electronics, vol. 64, no. 8, pp. 6202-6211, Aug. 2017, doi: 10.1109/TIE.2017.2677343.

[16] C. Yin, Z. Xin, L. Ming, and P. C. Loh, "Two Degrees of Freedom Power Decoupling Method for Single-Phase Split-Source Inverter," 2019 IEEE Applied Power Electronics Conference and Exposition (APEC), 2019, pp. 290-296, doi: 10.1109/APEC.2019.8722288.

[17] N. Güler, "Proportional Resonant and Proportional Integral Based Control Strategy for Single-Phase Split Source Inverters," 2020 9th International Conference on Renewable Energy Research and Application (ICRERA), 2020, pp. 510-514, doi: 10.1109/ICRERA49962.2020.9242690.

[18] A. A. Abd-Elaziz, S. M. Dabour, M. F. Elmorshedy, and E. M. Rashad, "Modeling and Control Of Stand-Alone Photovoltaic System Based On

Split-Source Inverter," 2021 22nd International Middle East Power Systems Conference (MEPCON), 2021, pp. 469-476, doi: 10.1109/MEPCON50283.2021.9686249.

[19] S. Kouro, P. Cortes, R. Vargas, U. Ammann, and J. Rodriguez, "Model predictive control - a simple and powerful method to control power converters," *IEEE Trans. on Ind. Electron.*, vol. 56, no. 6, pp. 1826-1838, June 2009.

[20] J. de Azevedo Borges and F. B. Grigoletto, "Finite set model predictive control of grid-connected split-source inverters," 2017 Brazilian Power Electronics Conference (COBEP), 2017, pp. 1-6, doi: 10.1109/COBEP.2017.8257297.

[21] M. A. Ismeil, "High Dynamic Performance for Split-Source Inverter based on Finite Control Set Model Predictive Control," 2019 21st International Middle East Power Systems Conference (MEPCON), 2019, pp. 8-13, doi: 10.1109/MEPCON47431.2019.9007972.

[22] G. M. Cocco, J. d. A. Borges, M. Stefanello and F. B. Grigoletto, "Finite Set Model Predictive Control of Four-Leg Split-Source Inverters," 2018 13th IEEE International Conference on Industry Applications (INDUSCON), 2018, pp. 630-635, doi: 10.1109/INDUSCON.2018.8627303.

[23] Y. Elthokaby, I. Mohamed, and N. Abdel-Rahim, "Model Predictive Control for Three-Phase Split-Source Inverter," 2020 22nd European Conference on Power Electronics and Applications (EPE'20 ECCE Europe), 2020, pp. 1-10.

[24] W. M. Abou-Hussein, S. M. Dabour, M. S. Hamad, and E. M. Rashad, "Model Predictive Control for Three-Phase Split-Source Inverter-Based Virtual Synchronous Generator," 2021 22nd International Middle East Power Systems Conference (MEPCON), 2021, pp. 648-653, DOI: 10.1109/MEPCON50283.2021.9686236.

[25] N. Guler and H. Komurcugil, "Energy Function-Based Finite Control Set Predictive Control Strategy for Single-Phase Split Source Inverters," in IEEE Transactions on Industrial Electronics, vol. 69, no. 6, pp. 5669-5679, June 2022, doi: 10.1109/TIE.2021.3090715.

[26] A. Bakeer, G. Magdy, A. Chub, and D. Vinnikov, "Predictive control based on ranking multi-objective optimization approaches for a quasi-Z source inverter," in CSEE Journal of Power and Energy Systems, vol. 7, no. 6, pp. 1152-1160, Nov. 2021, doi: 10.17775/CSEEJPES.2020.01310.